ACS MATERIALS Au
AN OPEN ACCESS JOURNAL OF THE AMERICAN CHEMICAL SOCIETY

pubs.acs.org/materialsau Article

# Structural and Morphological Properties of Wool Keratin and Cellulose Biocomposites Fabricated Using Ionic Liquids

Karleena Rybacki, Stacy A. Love, Bailey Blessing, Abneris Morales, Emily McDermott, Kaylyn Cai, Xiao Hu, and David Salas-de la Cruz*

Cite This: ACS Mater. Au 2022, 2, 21−32 Read Online

ACCESS | Metrics & More | Article Recommendations | Supporting Information

**ABSTRACT:** In this study, the structural, thermal, and morphological properties of biocomposite films composed of wool keratin mixed with cellulose and regenerated with ionic liquids and various coagulation agents were characterized and explored. These blended films exhibit different physical and thermal properties based on the polymer ratio and coagulation agent type in the fabrication process. Thus, understanding their structure and molecular interaction will enable an understanding of how the crystallinity of cellulose can be modified in order to understand the formation of protein secondary structures. The thermal, morphological, and physiochemical properties of the biocomposites were investigated by Fourier transform infrared (FTIR) spectroscopy, scanning electron microscopy (SEM), thermal gravimetric analysis (TGA), differential scanning calorimetry (DSC), and X-ray scattering. Analysis of the results suggests that both the wool keratin and the cellulose structures can be manipulated during dissolution and regeneration. Specifically, the $\beta$-sheet content in wool keratin increases with the increase of the ethanol solution concentration during the coagulation process; likewise, the cellulose crystallinity increases with the increase of the hydrogen peroxide concentration via coagulation. These findings suggest that the different molecular interactions in a biocomposite can be tuned systematically. This can lead to developments in biomaterial research including advances in natural based electrolyte batteries, as well as implantable bionics for medical research.

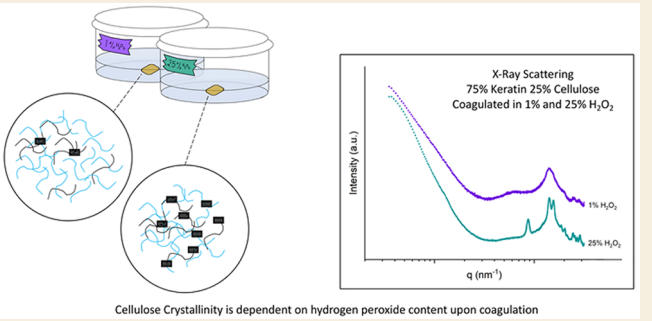

Cellulose Crystallinity is dependent on hydrogen peroxide content upon coagulation

**KEYWORDS:** *wool keratin, cellulose, biocomposite, ionic liquids, β-sheet content, crystallinity*

## INTRODUCTION

Advances in biomaterial research continue to be a growing topic of interest due to the increasing number of versatile and beneficial applications. These applications include tissue engineering, the filtering of heavy metals from the environment, drug delivery, sustainable food storage material, and the manufacture of natural based electrolyte batteries.[1−3] Biomaterials have favorable properties as they are biocompatible, inexpensive, and plentiful in the environment and have tunable physical and morphological properties.[1,4,5] For example, incorporating biomaterials into the production of scaffolds can aid in the potential for more therapeutic treatments in the field of tissue engineering as the natural materials can act as a guide for new tissue reformation, especially by tuning its mechanical properties (i.e., stiffness).[5,6] Another application of biomaterial research is within the fabrication of biomaterial-based and biodegradable transient implantable medical bionics (TIMBs).[7,8] The tuning of biomaterial physiochemical and morphological properties within TIMBs is a necessary component in order to design safe and effective devices. Even though biomaterials have been utilized successfully in these fields, the relationship between structure, morphology, and physicochemical properties is lacking.

Proteins are an ideal biomaterial to study as they are biodegradable, low in toxicity, and have tunable physical and morphological properties.[9] Protein materials commonly used in biocomposites include silk, keratin, soy, collagen, gelatin, resilin, corn zein, and wheat gluten. Polysaccharides are constructed from monomeric sugars that are joined together by glycosidic linkages and can store materials, compose structural components, and act as protective agents. Typical polysaccharides include starch, cellulose, pectin, alginates, chitin, chitosan, and hyaluronic acid found in plants, algae, or animals. Structural proteins and polysaccharide polymers interact through hydrophobic and electrostatic interactions,[10] and the resulting matrices formed by the mixture can exhibit

Received: May 20, 2021
Published: October 25, 2021

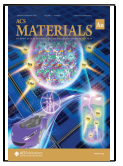





https://doi.org/10.1021/acsmaterialsau.1c00016
ACS Mater. Au 2022, 2, 21−32

useful and novel properties.[11−14] For example, Love et al. showed that the thermal and morphological properties of silk and cellulose biocomposites were dependent on the fabrication methods.[2] It was found that the cellulose crystal size can be manipulated via the coagulation process without affecting the resulting silk secondary structures. Blessing et al. further studied these morphological changes and provided evidence to suggest that the physicochemical properties, especially the thermal stability and ionic conductivity, were dependent on morphology (i.e., cellulose crystallinity and silk secondary structures (i.e., $\beta$ sheet content)).[4] As noted, transforming natural resources from their native state to a more usable form is nontrivial as their properties and fabrication processes are the subject of intense scientific scrutiny.[15−24]

Previously, we reported that the cellulose crystallinity and protein secondary structures can be independently tuned in a cellulose and silk blend during fabrication.[2] In this study, we will characterize a new blended system composed of keratin azure and Avicel microcrystalline cellulose to understand if these morphological and physicochemical changes can be replicated in a different protein. Keratin is a strong and fibrous structural protein that has a tunable secondary structure, analogous to silk. It is one of the most abundant proteins among mammals, birds, and reptiles as it can be found in hair, wool, nails, feathers, and horns to help provide protection and strength.[25,26] Keratin also makes up the majority of organic waste from wool textile industries, which includes the low-quality wool fibers unfit to be spun and the byproducts of butcher companies such as animal hooves, nails, feathers, and horns.[27] The main reason is due to a high cost of isolation and purification without destroying the molecular weight of the natural polymer. This makes keratin a great material to study in biomaterial research since there is an excess amount available in nature and the textile industries alone that could replace synthetic polymers.[28] In this study, keratin azure, which is "dye-impregnated sheep's wool keratin", was utilized due to its tensile strength and tunable properties.[29] Keratin azure is composed of keratin fibers that are found in sheep wool. The protein keratin is a polypeptide chain that exists in two formations: $\beta$-sheets and $\alpha$-helices. However, $\beta$-sheets are mainly found in the keratin located in the feathers and claws of birds and reptiles. Characteristically, $\alpha$-helices are found in all vertebrates' hair, skin, and nails.[30−32] The formation of the polypeptide chains of keratin results in either the $\alpha$- or the $\beta$-type; the $\alpha$-keratin type is formed if these chains curl to produce helices, while the $\beta$-keratin type is formed if the chains bond together in a side-by-side formation.[31] Keratin of both types have strong formations and are one of the primary proteins found in the protective tissues of animals. Due to the low density of wool keratin fibers, the dissolution and subsequent coagulation into a gel-like matrix can be made possible.[3] However, its properties can be manipulated if mixed with a different polymer such as cellulose.[33]

Avicel microcrystalline cellulose can be utilized in the fabrication process of the biocomposite films to manipulate physicochemical properties. Interest in cellulose has increased over the years as it is one of the most abundant and versatile biomaterials on earth.[34] Cellulose is a linear polymer of glucose, consisting of two glucose sugar units connected by glycosidic linkages.[34,35] In nature, cellulose is found as Cellulose I, and when regenerated, it exists as Cellulose II. The regenerated form has both amorphous and crystalline regions, which has the ability to form strong inter- and intramolecular hydrogen bonding.[34] Cellulose consists of crystalline regions with strong glycosidic, intra- and intermolecular hydrogen bonds, attributing to its high chemical and mechanical stability.[35]

One of the drawbacks when using biomaterials like those of wool keratin and cellulose is that they are insoluble in most solvents, including water. Wool keratin strands require a strong solvent in order to break down the tight packing of the $\alpha$-helices and $\beta$-sheets present in the polypeptide structure.[36] A "greener" alternative to organic solvents is to use ionic liquids. Ionic liquids are nonflammable, have high thermal stability and high dissolution properties, and are reusable when regenerated.[34−37] Using an ionic liquid as the solvent with a strong anion group will allow for the complete dissolution of the protein and polysaccharide, as well as an increased amount of inter- and intramolecular interactions with each other.

In this study, two different concentration ratios of protein to polysaccharide were explored, including 25% and 75% wool keratin, with the remainder of each percentage attributed to the Avicel microcrystalline cellulose. After dissolution, the biocomposites were coagulated in 1% and 25% hydrogen peroxide, as well as 1% and 25% ethanol. The coagulation process serves as a way to regenerate the protein and polysaccharide while removing as much ionic liquid as possible. Specifically, this causes a significant removal of the ions from the dissolution process within the biocomposite into the coagulation agent.[38] Various characterization tests were performed in order to understand the composition and coagulation method effects upon the mechanical, thermal, and morphological properties. As wool keratin and cellulose are abundant in nature, blending these biomaterials together in ratios where one dominates over the other can indicate tunable properties from the fabrication method. The aim of this study is to gain a fundamental understanding of the effects the fabrication method can have on the inter- and intramolecular interactions within the biocomposite films. Looking into these interactions can also lead to an understanding of how the crystallinity of cellulose can be modified in order to understand the formation of protein secondary structures. A better understanding of the different properties as well as the physical and chemical interactions within the biocomposite films can lead to a multitude of versatile applications.

## MATERIALS AND METHODS

### Ionic Liquid

1-Ethyl-3-methylimidazolium acetate (95%) was purchased from Sigma-Aldrich. The ionic liquid was pretreated in a vacuum oven (30 inHg) at 50 °C for 24 h to increase the solubility of the solvent.

### Natural Materials

Keratin Azure was purchased from Sigma-Aldrich (K8500-5G), which originated from dye-impregnated sheep's wool. The keratin was in the form of blue wool fibers. The wool strands were cut into smaller pieces to allow for easy dissolution within the ionic liquid solvent. Avicel Microcrystalline cellulose pf 250 mm (Techware: Z26578-0) was acquired from Analtech. The cellulose was pretreated in the vacuum oven (30 inHg) at 50 °C for 24 h.

### Dissolution of Protein and Polysaccharide

The total mass of the sample was composed of 90% ionic liquid and 10% polymers. For the various ratios tested, the 10% of the total sample mass was divided by the corresponding ratio of protein to polysaccharide. The protein:polysaccharide ratios included 25:75 and 75:25. The pretreated ionic liquid was measured to be 90% by mass in a glass vial and placed into an 80 °C silica oil bath to ensure an even


https://doi.org/10.1021/acsmaterialsau.1c00016
ACS Mater. Au 2022, 2, 21−32

and consistent heating throughout the dissolution process. The wool keratin was cut into shorter strands and added to the vial first. Once the full dissolution of wool keratin was completed, using a magnetic stir bar, the cellulose was added in small portions. After the full dissolution of cellulose was completed, the solution was left to mix for 24 h at a constant temperature of 80 °C.

### Preparation of Regenerated Biocomposite Films

After 24 h of mixing, the blended protein−polysaccharide solution was then transferred to a 12 mm × 12 mm × 1 mm 3D printed mold made of polylactic acid. To ensure the solution did not solidify while pipetting into the mold, a 1 mL micropipette tip was heated to 75 °C 15 min prior to distribution. This also allowed for a seamless transfer of the blended solution into the molds after dissolution, avoiding the loss of material within the pipet tip due to high viscosity. After pipetting, the mold was transferred to a 250 mL beaker and submerged into 100 mL of the specific coagulation agent, either in a solution prepared with DI water and 1% or 25% ethanol and/or 1% or 25% hydrogen peroxide. The beaker was then sealed using parafilm for 48 h. During this time, the protein−polysaccharide solution was regenerated while removing as much of the remaining ionic liquid trapped within the blend as possible. After 48 h, the molds were removed from the coagulation baths, transferred to a closed Teflon Petri dish, and placed in a vacuum oven (30 inHg) at 50 °C for 24 h for complete dryness.

### Characterization Tests

**Fourier Transform Infrared (FTIR) Spectroscopy.** Fourier transform infrared (FTIR) spectroscopy analysis was performed using a Bruker's ALPHA-Platinum ATR-FTIR spectrometer with a platinum−diamond sample module. For each film, data was collected for a spectra range of 4000 $cm^{-1}$ to 400 $cm^{-1}$, including 128 background scans and 32 sample scans. This was completed for 6 different locations on the film, and an average spectrum was collected. The amide I region (1705−1595 $cm^{-1}$) was studied using Fourier self-deconvolution with a Lorentzian line shape, a 25.614 $cm^{-1}$ half-bandwidth, and a noise reduction factor of 0.3. The program Opus 7.2 was used to fit the peaks that corresponded to the various vibrational band assignments of the protein secondary structures within the amide I region. To allow for fitting results, Gaussian profiles were utilized and then integrated to find the area relating to a specific wavelength. After analysis, the data was normalized using a min−max normalization from 4000 to 400 $cm^{-1}$ to better show the functional groups within the spectra.

**Scanning Electron Microscopy (SEM).** Scanning Electron Microscopy (SEM) was performed using the Jeol JCM-6000 SEM instrument to analyze the topographical properties of the regenerated films. Images were taken at 500× magnification with a scale of 100 mm. The films were cut into rectangular pieces and coated using a DII-29010SCTR Smart Coater at vacuum level 4 Pa. The samples were coated in Au−Pt for 60 s.

**Thermogravimetric Analysis (TGA).** Thermogravimetric analysis (TGA) was performed using the TA Instruments Discovery TGA Q600 SDT system. All tests were performed with ∼5 mg samples under a nitrogen gas purge of 25 mL/min initially starting at 30 °C and kept isothermal at this temperature for 1 min. The 5 mg samples were heated using a 10 °C/min ramp until the temperature was at 600 °C. Step transition analysis and derivative plots were used to determine the temperature of the onset of decomposition ($T_{onset}$) and the weight-loss percentage of the sample. Peak height analysis was performed to determine the temperature at which the sample decomposed at the highest rate ($T_{Dmax}$).

**Differential Scanning Calorimetry (DSC).** Differential scanning calorimetry (DSC) was performed using the TA Instruments differential scanning calorimetry equipped with a refrigerated cooling system via a nitrogen gas flow rate of 50 mL $min^{-1}$. The ∼5 mg samples were enclosed in aluminum Tzero pans. The calibration process included indium for heat flow and temperature. The modulated procedure for DSC measurements included an equilibration to −40 °C, a modulation period of 60 s with a temperature amplitude of 0.318 °C, isothermal for 3 min, and an increase in temperature of 2 °C/min to 400 °C. The calibration of the heat flow and heat capacity was completed using aluminum and sapphire reference pans.[39] The glass transition temperatures ($T_g$) were calculated from the reversing heat capacity thermograms.

**X-ray Scattering.** The morphological studies were conducted using a multiangle X-ray scattering system (DEXS) at the University of Pennsylvania under vacuum. The Xeuss 2.0 by XENOCS has a Cu X-ray source, computer controlled focusing and transmission incident sample geometries, a 1 M pixel Pilatus detector (2D), and a smaller detector for simultaneous SAXS and WAXS acquisition. A high flux collimation was used with a slit of 1.2 mm × 1.2 mm. Samples containing a greater amount of keratin were run for 600 s while the samples containing a greater amount of cellulose were run for 300 s. The intensity reported is not absolute intensity and, thus, is reported in arbitrary units (a.u.). All samples were taped to a sample holder and placed in a cabin under vacuum during X-ray scattering characterization. The X-ray scattering profiles were evaluated using Foxtrot 3.4.9; the isotropic 2-D scattering patterns were azimuthally integrated to yield profiles of scattering vector ($q$) versus intensity.

## RESULTS AND DISCUSSION

Analysis of the data obtained from the various polymer ratios and coagulation agent types used in polymer fabrication provided qualitative changes in sample physical properties, i.e., stiffness or flexibility. The regenerated films composed of a higher percentage of wool keratin and those coagulated in ethanol were more delicate, while those with a higher percentage of cellulose and those coagulated in hydrogen peroxide were more durable. The following characterization tests provided more information relating to the morphological and thermal properties when the protein to polysaccharide ratio and the coagulation agent type was varied.

### Fourier Transform Infrared Spectroscopy

Fourier transform infrared (FTIR) spectroscopy was performed to confirm that the proper mixing and regeneration of the polymer solution was achieved. This characterization test also allowed for the percentages of the protein secondary structures to be calculated. In Figure 1, the IR spectra were normalized to compare the peak positions for the multiple samples. The positions of the peaks remained constant in all of the IR spectra. The peaks visible in all spectra originating from cellulose within the regenerated films are the O−H stretch from approximately 3000 $cm^{-1}$ to 3550 $cm^{-1}$, the C−H stretch located at approximately 2900 $cm^{-1}$, and the C−O−C at 1000 $cm^{-1}$, as seen in Figure 1a. Additionally, all samples had a small shoulder peak at approximately 1160 $cm^{-1}$, which most likely corresponds to the C−N stretch found in the imidazolium ring, suggesting a miniscule amount of remaining ionic liquid within the film.

The peaks that correspond to the amide I and II regions are located from 1500 to 1700 $cm^{-1}$ and the amide III region is located around 1230 $cm^{-1}$. The amide regions originate from the wool keratin within the samples, as seen in Figure 1b. The characterized cellulose and wool keratin peaks show consistent peak positions for all spectra. When comparing between polymer ratio sets, the spectra of the films composed of 75% wool keratin and 25% cellulose, Figure 1b, had a sharper peak for the O−H stretch rather than a smooth, broader curve. This could be due to a lower percentage of cellulose and the higher percentage of wool keratin contributing, as seen in the spectrum of the initial samples, Figure 1. However, when comparing the coagulation agent type, the O−H stretch in the 25% hydrogen peroxide samples remained consistent with the smooth, broader curve. Overall, changes in the coagulation


https://doi.org/10.1021/acsmaterialsau.1c00016
ACS Mater. Au 2022, 2, 21−32

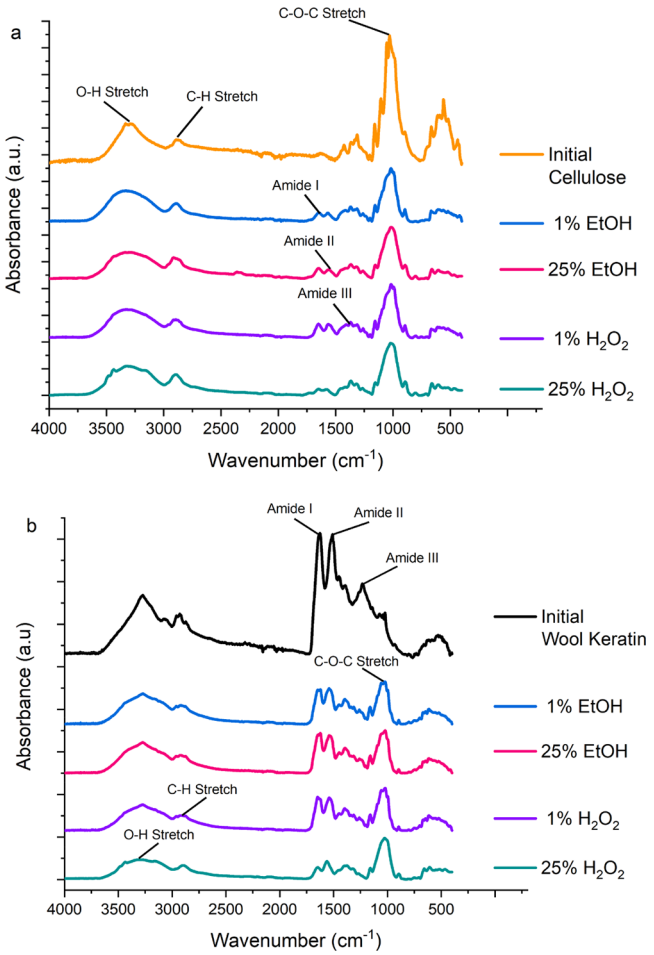


**Figure 1.** (a) FTIR spectra of initial cellulose with 25% wool keratin and 75% cellulose coagulated in 1% and 25% of ethanol and hydrogen peroxide and (b) initial wool keratin with 75% wool keratin and 25% cellulose films coagulated in the same coagulant. Supporting Information Figure S-1 shows the various amide regions for each composition and coagulation bath.

agent did not have any substantial effects on the resulting spectra due to the presence of all expected functional groups. Thus, we can conclude that both biomacromolecules are incorporated within the biocomposite matrix.

The amide I regions on the FTIR spectra, located from 1705−1595 $cm^{-1}$, of the initial wool keratin and the regenerated samples were analyzed using Fourier self-deconvolution.[40,41] Supporting Information Figure S-1 shows the various amide regions for each composition and coagulation bath. The calculated secondary structure percentages and each standard deviation are displayed in Table 1. For the initial wool keratin secondary structure percentages, the values were reasonably close to those from Vu et al.[41] In comparison, the secondary structure percentages of the regenerated films were also relatively close in value to the initial percentages for the initial wool keratin. Most of the films composed of 25% wool keratin and 75% cellulose had either approximately 1% or less side chains. The percentages of $\alpha$-helices in this ratio composition of wool keratin remained consistent and were unaffected by the changes in the coagulation bath type. However, in the 75% wool keratin and 25% cellulose films the side chains were greater than 1%, the largest reported value being 5.7% ± 3.1. The $\alpha$-helices for

**Table 1. Percentages of Secondary Structures and Corresponding Standard Deviations of Initial Wool Keratin and Wool Keratin/Cellulose Regenerated Films in Various Coagulation Bath Types**

| sample ratios | coagulant bath | side chains | $\beta$-sheets | random coils | $\alpha$-helices | turns |
|---|---|---|---|---|---|---|
| initial wool keratin | - | 5.2% | 33.0% | 29.1% | 8.7% | 23.9% |
| | | ±1.6 | ±1.3 | ±0.4 | ±0.1 | ±0.2 |
| 25% wool keratin and 75% cellulose | 1% EtOH | 1.2% | 27.7% | 43.1% | 12.0% | 16.1% |
| | | ±0.8 | ±5.8 | ±11.4 | ±5.4 | ±3.3 |
| | 25% EtOH | <1% | 28.4% | 28.7% | 16.3% | 26.3% |
| | | ±0.2 | ±3.8 | ±8.8 | ±1.5 | ±5.5 |
| | 1% $H_2O_2$ | <1% | 20.3% | 30.9% | 16.1% | 32.6% |
| | | ±0.8 | ±5.7 | ±6.3 | ±10.7 | ±3.6 |
| | 25% $H_2O_2$ | <1% | 18.4% | 36.3% | 16.0% | 29.1% |
| | | ±0.1 | ±6.7 | ±9.9 | ±12.8 | ±8.0 |
| 75% wool keratin and 25% cellulose | 1% EtOH | 4.1% | 31.6% | 30.9% | 2.9% | 30.6% |
| | | ±3.0 | ±3.9 | ±7.7 | ±6.1 | ±5.6 |
| | 25% EtOH | 3.1% | 33.6% | 23.2% | 5.1% | 35.0% |
| | | ±1.4 | ±4.5 | ±4.8 | ±4.6 | ±11.1 |
| | 1% $H_2O_2$ | 5.7% | 30.2% | 27.8% | 15.7% | 20.6% |
| | | ±3.1 | ±5.5 | ±5.6 | ±3.5 | ±3.5 |
| | 25% $H_2O_2$ | <1% | 22.9% | 13.5% | 34.3% | 29.3% |
| | | ±0.1 | ±6.8 | ±1.6 | ±12.7 | ±5.3 |

this composition increased as the percentages of the coagulation baths also increased. This indicates that when the percentage of keratin dominates in the composite, the coagulation agent, especially hydrogen peroxide, can also promote the protein chains to a form more ordered structure, such as from random coils to helical structures.

The highest secondary structure content calculated within the FTIR data was $\beta$-sheets, random coils, and turns. Previous studies report that increasing the percentage of ethanol used as the coagulation agent caused an increase in the resulting $\beta$-sheet percentage within the regenerated sample.[4] This trend is also present in this study as the percentage of ethanol increases; the $\beta$-sheet content also increases by 0.7% and 2.0% for the 25% and 75% wool keratin composition films, respectively. As the percentage of hydrogen peroxide increased, an inverse relationship was exhibited, and the $\beta$-sheet percentage decreased. Overall, the films coagulated in 25% ethanol had the highest percentage of $\beta$-sheets while the film coagulated in 25% hydrogen peroxide had the lowest $\beta$-sheet percentage. Also, the higher percentage of keratin present resulted in an overall higher percentage of beta sheets.

The films with 25% wool keratin had more random coils than the 75% wool keratin films. When the percentage of ethanol was increased, the resulting percentage of random coils decreased. This change was very apparent in the 25% wool keratin films as the maximum difference was 14.4%, while in the 75% keratin films the difference was 7.7%. The percentage of turns varied the most for the 25% wool keratin samples regenerated in ethanol and 75% wool keratin samples regenerated in hydrogen peroxide. The calculation of the secondary structure content helped to provide more insight into the protein crystalline and amorphous regions of the blended films.

## Scanning Electron Microscopy (SEM)

Scanning Electron Microscopy was performed to illustrate the morphological effects upon the topography of the regenerated films and is shown in Figure 2 and Figure 3. As a function of


https://doi.org/10.1021/acsmaterialsau.1c00016
ACS Mater. Au 2022, 2, 21−32

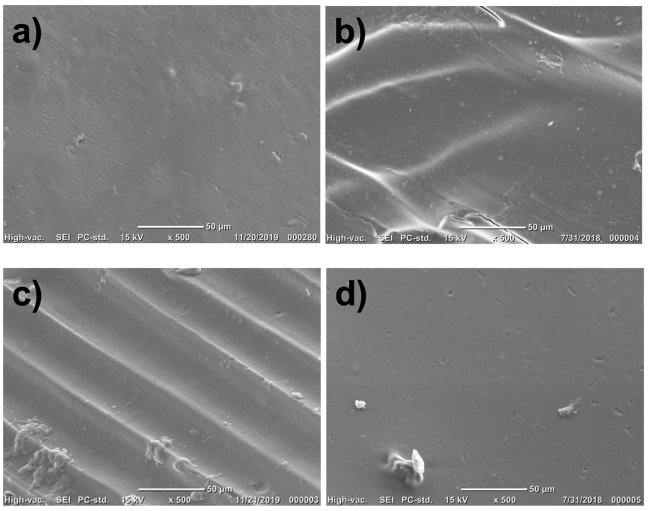


**Figure 2.** SEM images of 25% wool keratin and 75% cellulose regenerated films at 500× magnification: (a) 1% ethanol, (b) 25% ethanol, (c) 1% hydrogen peroxide, and (d) 25% hydrogen peroxide.

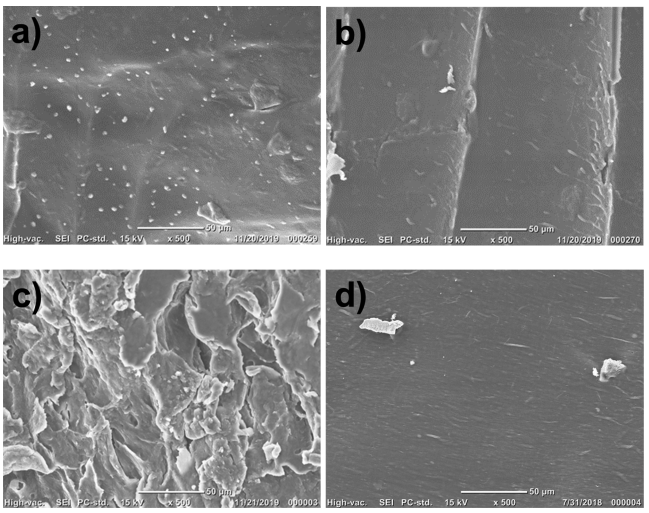


**Figure 3.** SEM images of 75% wool keratin and 25% cellulose regenerated films at 500× magnification, (a) 1% ethanol, (b) 25% ethanol, (c) 1% hydrogen peroxide, and (d) 25% hydrogen peroxide.

protein percentage, the regenerated films with 25% wool keratin were shown to have an overall smoother surface. The films appeared mostly homogeneous, suggesting the proper blending and regeneration of the polymers; however, there were some areas of irregularities with visible cellulose particles on the surface. The regenerated films with 75% wool keratin were shown to have more prominent areas of "roughness", particularly seen in the sample coagulated in the lower hydrogen peroxide concentration, Figure 3c. The ethanol samples had a more consistent and smoother surface, Figure 3a,b. As the percentage of the coagulation agent increased, the resulting films had a smoother surface. Some of the films exhibited striations that ran the entire length of the film. This was considered to be an artifact of the system, which was a result of the mold in which the films were regenerated and dried.

## Thermogravimetric Analysis

Thermogravimetric analysis (TGA) was performed to determine the decomposition properties of the various biocomposite films. This was achieved through the comparisons of the different weight loss percentages, as well as the onset, end, and maximum temperatures of decomposition; all values are listed in Table 2. The analysis of the resultant

**Table 2. Onset and End Temperatures, Total Weight Loss Percentage, and Maximum Temperature of Decomposition Given by the Derivative that Represents the Temperature at Which the Maximum Weight Loss Occurred**

| sample ratios | coagulant bath | $T_{Onset}$ (°C) | $T_{End}$ (°C) | weight loss (%) | $T_{\Delta Max}$ (°C) |
|---|---|---|---|---|---|
| initial wool keratin | - | 261.8 | 352.1 | 64.0% | 309.8 |
| initial cellulose | - | 334.7 | 364.8 | 86.4% | 352.2 |
| 25% wool keratin and 75% cellulose | 1% EtOH | 220.0 | 315.1 | 66.1% | 241.8 |
| | | | | | 321.4 |
| | 25% EtOH | 229.7 | 324.1 | 61.8% | 252.8 |
| | | | | | 337.9 |
| | 1% $H_2O_2$ | 216.4 | 297.8 | 65.8% | 233.0 |
| | | | | | 282.0 |
| | 25% $H_2O_2$ | 224.9 | 332.2 | 63.8% | 253.8 |
| | | | | | 335.9 |
| 75% wool keratin and 25% cellulose | 1% EtOH | 239.1 | 327.2 | 67.2% | 288.6 |
| | 25% EtOH | 253.6 | 330.0 | 67.5% | 291.3 |
| | 1% $H_2O_2$ | 252.7 | 326.9 | 65.5% | 289.3 |
| | 25% $H_2O_2$ | 215.7 | 317.2 | 70.5% | 277.0 |

thermograms and respective derivative weight-loss percentage thermograms also gave insight into the thermal and molecular properties of the films. The thermograms, Figures 4 and 5, show the sample weight loss percentage during a constant increase of temperature from 30−600 °C. Similar to the study from Li et al., the initial weight loss between 50 to 100 °C could be attributed to the loss of water, whereas the weight loss between 175−500 °C was most likely representative of the decomposition of wool keratin and cellulose chains.[42] The samples with higher keratin content had a greater weight loss percentage and slightly higher onset temperatures than samples with more cellulose, except for the sample coagulated in 25% hydrogen peroxide.

The time it took for samples to fully degrade is in relation to the range between the onset and end temperatures. The 75% wool keratin films had a smaller temperature range and quicker degradation, for full sample degradation, in comparison to the 25% wool keratin films. Thermograms of samples with a higher percentage of cellulose degraded over a larger temperature range, as cellulose itself is more thermally stable than wool keratin, showing the influence the protein has on the thermal stability. As a function of the coagulation bath type, the onset temperatures increased as the concentration of ethanol and hydrogen peroxide solutions increased. Only the thermogram of 75% wool keratin films regenerated in 25% hydrogen peroxide solution showed to have an inverse relationship, i.e., a lower onset temperature. Overall, the protein and polysaccharide content, choice of coagulation bath type, and percent concentration resulted in subtle but noticeable changes to the thermal properties.

Derivative thermograms show the maximum temperatures of degradation ($T_{\Delta Max}$), and analysis of $T_{\Delta Max}$ gives insight into the interfaces of the molecular structure.[4] The 75% wool keratin samples' derivative thermograms illustrated unimodality with small shoulder peaks before the maximum


https://doi.org/10.1021/acsmaterialsau.1c00016
ACS Mater. Au 2022, 2, 21−32

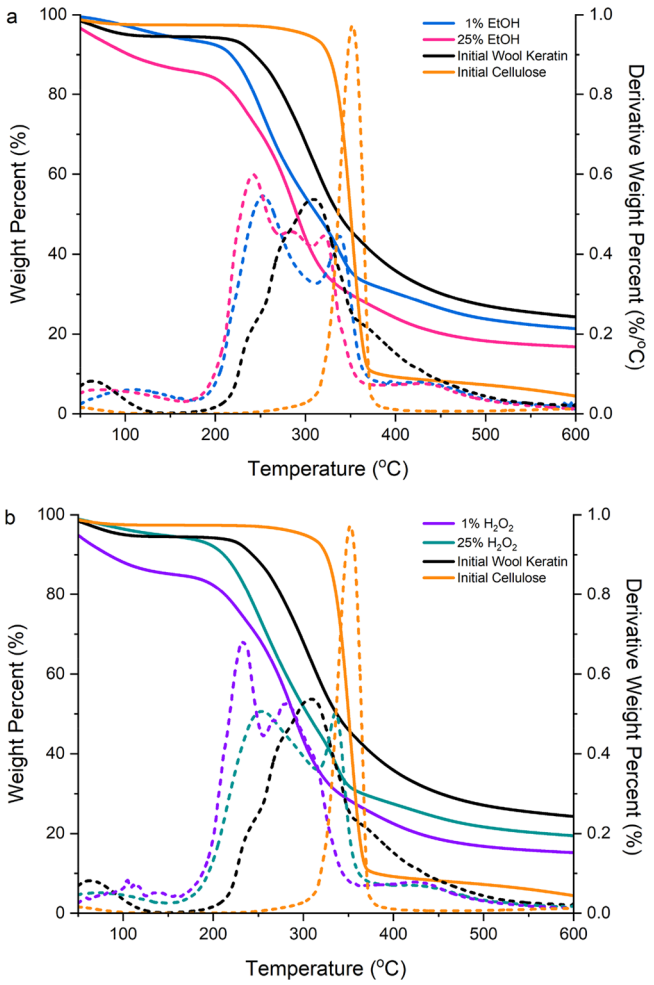


**Figure 4.** Thermograms of 25% wool keratin and 75% cellulose in (a) ethanol and (b) hydrogen peroxide coagulation agents with the corresponding derivative thermograms.

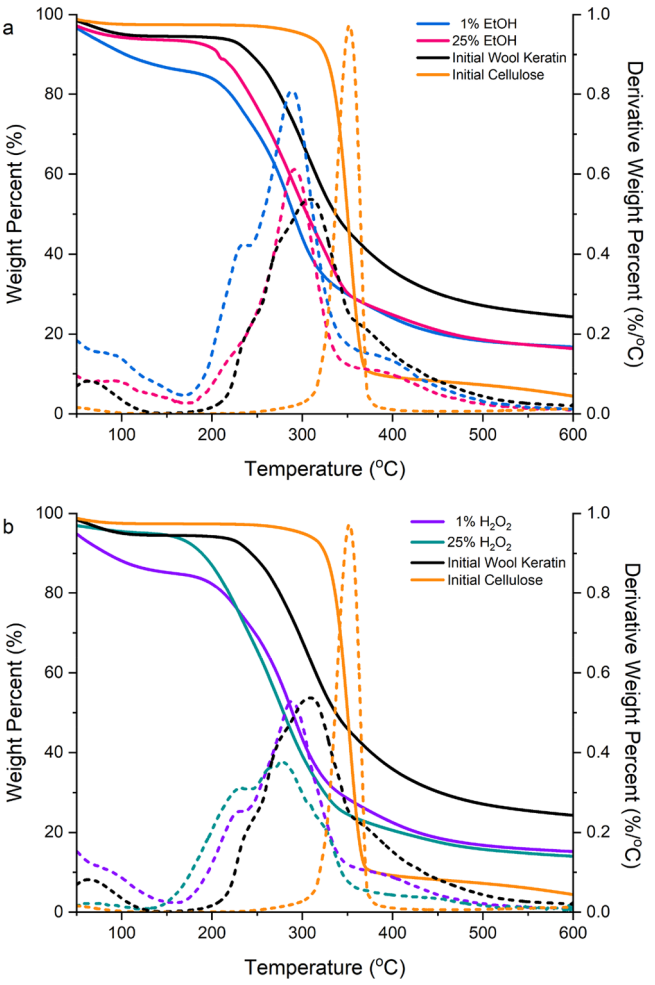


**Figure 5.** Thermograms of 75% wool keratin and 25% cellulose in various (a) ethanol and (b) hydrogen peroxide coagulation agents and the corresponding derivative thermograms.

temperature. The shoulder peak could be interpreted to be the degradation of the amorphous protein secondary structures at a lower temperature. The 75% wool keratin samples also had a relatively smaller percentage of amorphous secondary structures and an overall higher percentage of crystalline secondary structures. The unimodal peaks, $T_{\Delta Max}$, and broadness of the derivatives resembled that of the initial wool keratin derivative. This further proves proper regeneration of wool keratin within the blends, as well as the concept that 75% wool keratin blended films followed a similar trend to that of the initial wool keratin. On the contrary, the 25% wool keratin derivative thermograms showed multimodality. The secondary structure content of these films was calculated to have a slightly lower percentage of $\beta$-sheets and an overall higher percentage of amorphous secondary structures i.e., random coils and turns. This difference in structure morphologies could be the cause of the bimodal and trimodal characteristics in the derivative thermograms. In other words, the amorphous structures degraded at lower temperatures than the crystalline regions, and thus the samples' profiles had multiple $T_{\Delta Max}$ values.

The thermal stability of the regenerated keratin samples decreased compared to the initial wool keratin. This could be due to the changes in the molecular structure during the dissolution and subsequent regeneration of the protein. The intermolecular forces which hold the polymer chains together were disrupted by the ionic liquid forces during dissolution, causing a less ordered and stable structure than the initial polymers, proving the significant role that solvation can have on the thermal properties of the samples.[42]

## Differential Scanning Calorimetry (DSC)

In Figure 6 and Figure 7, standard DSC scans are shown for different samples of various wool keratin/cellulose percentages using solutions of ethanol and hydrogen peroxide as coagulation agents and EMIMAc as the ionic liquid. In Figure 6a,b, the endothermic (water peak) and crystallization peaks (exothermic peaks) were determined using the total heat flow. In the 25% wool keratin samples, Figure 6a, 1% ethanol and 25% hydrogen peroxide samples had an endothermic peak at approximately 70 and 65 °C, respectively. This endothermic peak is related to water retention. In the TGA section, we showed weight loss between 50 to 100 °C is attributed to the loss of water. The 1% hydrogen peroxide sample had this water peak located at a higher temperature of approximately 85 °C, while the 25% ethanol sample seemed to have had only a slight peak, much less defined and shifted to a higher temperature of approximately 95 °C. These samples also had two crystallization peaks with the first between 215 and 225 °C and the second between 295 and 300 °C. These exothermic peaks result from their initial material degradation as shown in the


https://doi.org/10.1021/acsmaterialsau.1c00016
ACS Mater. Au 2022, 2, 21−32

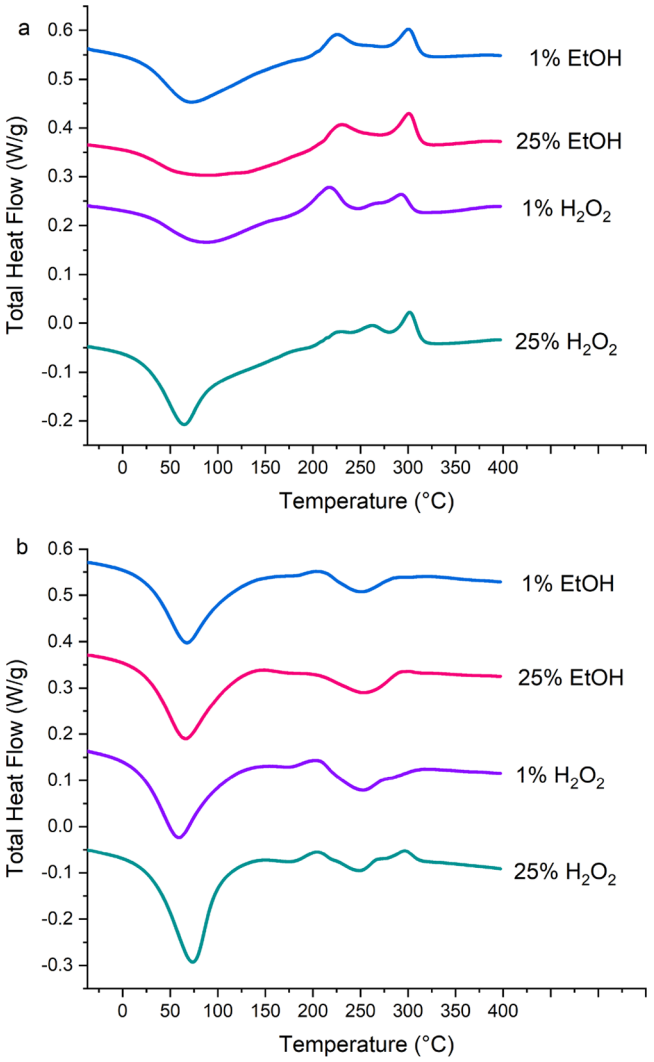


**Figure 6.** (a) 25% wool keratin and 75% cellulose standard DSC scans and (b) 75% wool keratin and 25% cellulose scans. These scans are used to show crystallization and degradation peaks in the samples.

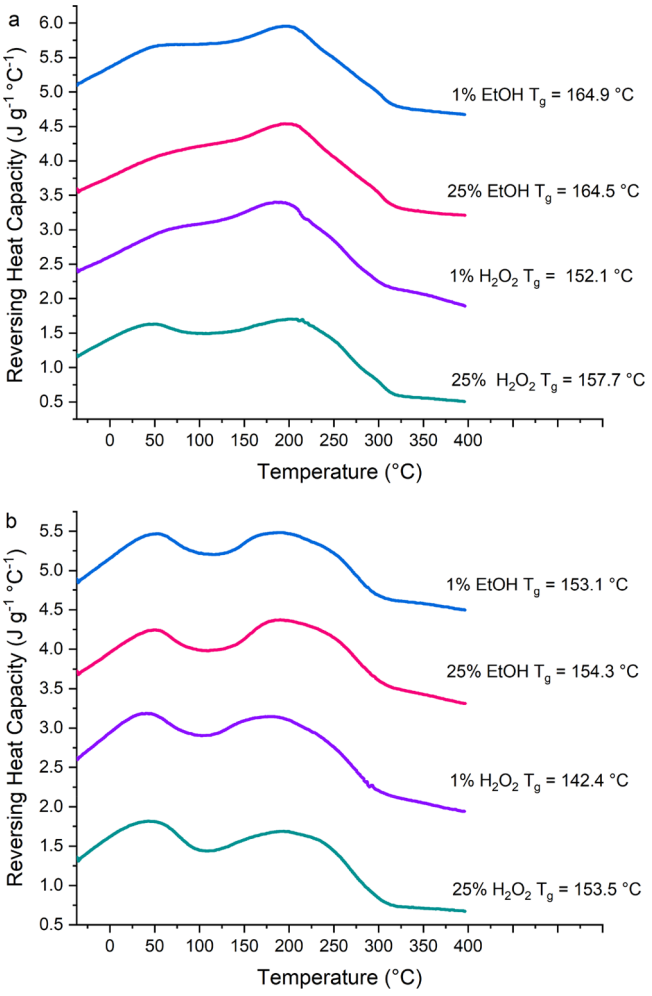


**Figure 7.** (a) 25% wool keratin and 75% cellulose reversing heat capacities and (b) 75% wool keratin 25% cellulose reversing heat capacities. These scans are used to obtain the glass transition temperature ($T_g$) of all eight samples, listed next to their respective graph.

TGA section. However, the 25% hydrogen peroxide did not have a well-defined first crystallization peak like the other three samples above it. Instead, it seems that there may have been two smaller crystallization peaks before the third much sharper peak that lined up with the other samples. These 25% wool keratin samples differed from the 75% wool keratin samples in that the 75% wool keratin samples seemed to have the water peaks and minimal distinct crystallization peaks (exothermic peak). Again, there was a large water peak that ranged from approximately 60 to 72 °C depending on the specific sample analyzed. This was followed by a second and much smaller crystallization peak at 200 °C and a melting peak at approximately 250 °C for each of the four samples. It is important to remember that the samples started to degrade at 200 °C as shown in the TGA section. When looking at the scans for all four samples, the 1% and 25% hydrogen peroxide samples looked as if they may have had one and two very small crystallization peaks respectively after 250 °C. This may suggest that the percentage of cellulose had some effects on the system in terms of thermal stability. It could also suggest that secondary crystalline structures are melting, and recrystallization is occurring before or after initial material degradation which is affected by morphology.

In Figure 7a,b, the glass transition temperatures ($T_g$) were determined using the reversing heat capacities. In the 25% wool keratin samples, Figure 7a, it was seen these temperatures did not vary drastically from sample to sample. Specifically, there was only a 12.7 °C difference from the highest to lowest $T_g$ corresponding to the 1% ethanol and 1% hydrogen peroxide samples, respectively. This differed from the 75% wool keratin samples where nearly all samples were the same except for the 1% hydrogen peroxide sample. The 1% ethanol, 25% ethanol, and 25% hydrogen peroxide samples had a glass transition temperature that only varied by 1.1 °C. However, the 1% hydrogen peroxide had a much lower glass transition temperature than these three samples, which was 11.8 °C lower than the highest glass transition temperature belonging to the 25% ethanol sample. When comparing samples of the same coagulation agent but different biocomposite ratios, it was seen that the 25% wool keratin samples had higher glass transition temperatures for each coagulant. In addition, when comparing the coagulation agents within the same biocomposite ratios, 1% and 25% ethanol glass transition temperatures had less variation than the 1% and 25% hydrogen peroxide


https://doi.org/10.1021/acsmaterialsau.1c00016
ACS Mater. Au 2022, 2, 21−32

samples. This may have been connected to the secondary structures discussed in the FTIR section. The $\beta$-sheet content varied less between the 1% and 25% ethanol of the same biocomposite ratio than the 1% and 25% hydrogen peroxide of the same biocomposite ratio.

### X-ray Scattering

X-ray small-angle scattering (SAXS) and wide-angle scattering (WAXS) were performed for the morphological comparison of the initial wool keratin and microcrystalline Avicel cellulose to regenerated wool keratin-cellulose blended biomaterials; refer to Figure 8 for the 1-D profiles of all initial materials and

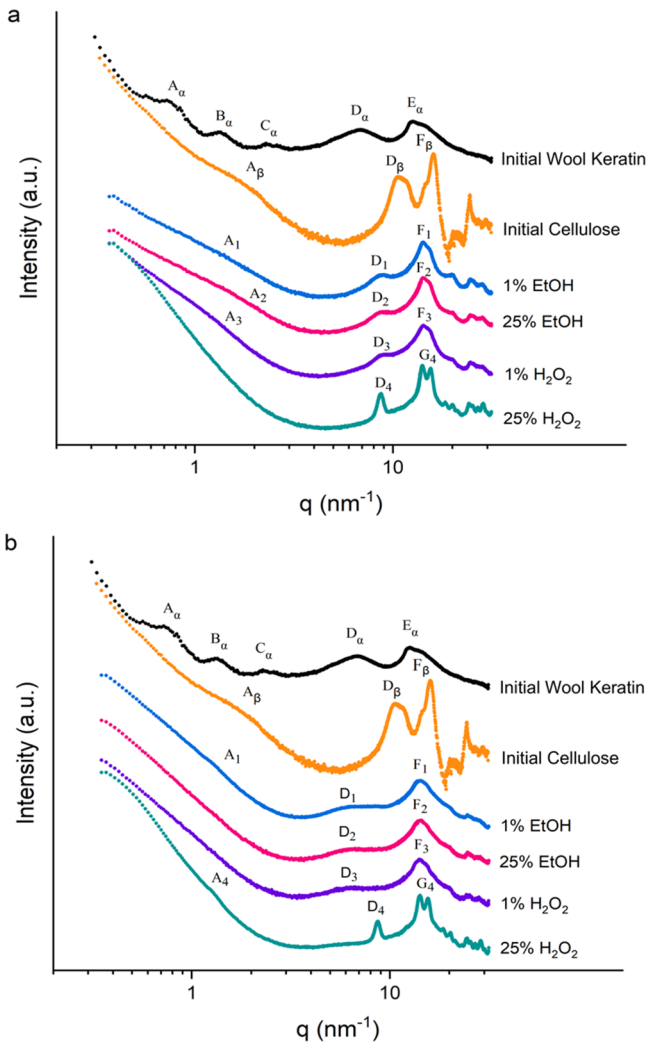


**Figure 8.** X-ray scattering profiles of the initial wool keratin, initial cellulose, and biocomposite films regenerated in various coagulant baths (listed on legend): (a) 25% wool keratin and 75% cellulose and (b) 75% wool keratin and 25% cellulose.

samples. Figure 8a shows biomaterials composed of 25% wool keratin and 75% cellulose, all of which were fabricated using the solvent, EMIMAc, and coagulation agents: ethanol or hydrogen peroxide solutions (1 and 25 vol % in $H_2O$). Interpretation of the qualitative analysis was that the reflection regions shown in the profiles of the regenerated samples labeled as $A_n$, $D_n$, and $F_n$ are characteristic of the reflection regions labeled on the initial materials' profiles, $A_{\alpha,\beta}$, $D_{\alpha,\beta}$, and $F_{\alpha,\beta}$. Furthermore, when compared to these initial materials, the aforementioned reflections in the regenerated sample profiles not only are shifted along the scattering vector ($q$) but also showed varying degrees of peak broadness and/or sharpness in intensity. These shape variations of peaks and shifts along the scattering vector were most likely due to changes in the intermolecular exchanges within the materials' matrix, e.g., wool keratin secondary structures interacting with cellulose crystallites. Similar results are shown in Figure 8b (75% wool keratin to 25% cellulose), and all $q$ and $d$ values for WAXS and SAXS are shown in Table 3.

In Figure 8a, the 25% wool keratin samples' peaks $D_n$ and $F_n$ are characteristic of reflections generated by the cellulose within the fabricated samples. The rationale for this was extrapolated from previous work where similar peaks appeared in regenerated biomaterials comprised of 100% Avicel cellulose, as well as blended biomaterials containing a different protein, silk fibroin.[2] When comparing the regenerated samples consisting of 75% wool keratin, Figure 8b, to the opposing polymer ratio set, the peak denoted as $D_n$ shifts to a decreased $q$ value and broadens in intensity; this peak muting was most likely due to the initial wool keratin (refer to $D_\alpha$). However, in the profiles of the 25% hydrogen peroxide coagulated samples from both polymer ratio sets, another noticeable difference in the WAXS region may be observed. A bimodal peak labeled as $G_4$ appears regardless of polymer ratio content. Analysis of this distinctive doublet reveals an overall increase in cellulose crystallinity due to an increased amount of hydrogen peroxide molecules. The theory is that, upon fabrication, hydrogen peroxide molecules have the ability to hydrogen bond with cellulose hydroxide groups, thus aligning the molecules in solution and later enhancing more crystalline-type cellulose structures. This process may have been due to the hydrogen peroxide converting to oxygen gas and water molecules in situ, which collapsed the polymer chains and resulted in changes of polysaccharide microcrystallinity.[2]

In regard to the peaks denoted as $F_n$, a similar reflection shift may be seen irrespective of polymer ratio content in all sample profiles minus those of the 25% hydrogen peroxide coagulated films where the peak ($G_4$) appears as a doublet. This shift in scattering vector may have been due to a combined effect from both cellulose and wool keratin. However, such peaks are more pronounced in the 25% wool keratin samples when compared to the reversed polymer ratio set and were most likely due to a greater content of cellulose within the blends. The rationale is that, when considering the X-ray scattering profiles of the initial cellulose, the distribution of sharper and larger peaks in that general area reflect greater changes in crystallinity and, thus, would more greatly influence the crystal structure within that plane.

The equation $d = 2\pi/q$ was used to calculate the crystalline interplanar spacing ($d$-spacing) for all materials within this study, and all values are located in Table 3. Due to the reciprocal relationship of $d$ and $q$ (scattering vector), the distance between atoms in a crystalline lattice decreases as $q$ increases, and reflections A, D, F, and G were analyzed quantitatively in this work. Upon investigating WAXS data starting at the $D_n$ site, which provides information on the subnanometer-sized structures, $d$ values at any particular plane were more similar to those calculated from the polymer that dominated in the respective regenerated sample. For example, the $d$-spacing values calculated for the $D_n$ peak in the 75% wool keratin profiles more closely matched the $d$ values calculated for the peak labeled as $D_\alpha$ (initial wool keratin). Though one exception was that of the 75% wool keratin sample regenerated


https://doi.org/10.1021/acsmaterialsau.1c00016
ACS Mater. Au 2022, 2, 21−32

Table 3. Peak $q$ and $d$ Values in Inverse Nanometers Calculated from X-ray Scattering 1-D Profiles for Initial Materials and Biocomposite Samples

| | | A | | B | | C | | D | | E | | F | | G | |
|---|---|---|---|---|---|---|---|---|---|---|---|---|---|---|---|
| sample ratio | coagulant bath | $q$ ($nm^{-1}$) | $d$ (nm) | $q$ ($nm^{-1}$) | $d$ (nm) | $q$ ($nm^{-1}$) | $d$ (nm) | $q$ ($nm^{-1}$) | $d$ (nm) | $q$ ($nm^{-1}$) | $d$ (nm) | $q$ ($nm^{-1}$) | $d$ (nm) | $q$ ($nm^{-1}$) | $d$ (nm) |
| initial wool keratin | - | 0.77 | 8.21 | 1.34 | 4.68 | 2.29 | 2.74 | 6.79 | 0.93 | 12.39 | 0.51 | - | - | - | - |
| initial cellulose | - | 1.95 | 3.22 | - | - | - | - | 10.55 | 0.6 | | | 15.98 | 0.39 | - | - |
| 25% wool keratin and 75% cellulose | 1% EtOH | 1.44 | 4.37 | - | - | - | - | 8.64 | 0.73 | - | - | 14.18 | 0.44 | - | - |
| | 25% EtOH | 1.49 | 4.21 | - | - | - | - | 8.52 | 0.74 | - | - | 14.18 | 0.44 | - | - |
| | 1% $H_2O_2$ | 1.44 | 4.37 | - | - | - | - | 8.64 | 0.73 | - | - | 14.18 | 0.44 | - | - |
| | 25% $H_2O_2$ | - | - | - | - | - | - | 8.75 | 0.72 | - | - | - | - | 13.98 | 0.45 |
| | | | | | | | | | | | | | | 15.56 | 0.4 |
| 75% wool keratin and 25% cellulose | 1% EtOH | 1.31 | 4.81 | - | - | - | - | 5.93 | 1.06 | - | - | 14.18 | 0.44 | - | - |
| | 25% EtOH | - | - | - | - | - | - | 6.35 | 0.99 | - | - | 14.36 | 0.44 | - | - |
| | 1% $H_2O_2$ | - | - | - | - | - | - | 5.93 | 1.06 | - | - | 14.18 | 0.44 | - | - |
| | 25% $H_2O_2$ | 1.29 | 4.87 | - | - | - | - | 8.64 | 0.73 | - | - | - | - | 14.36 | 0.44 |
| | | | | | | | | | | | | | | 15.78 | 0.4 |

in 25% hydrogen peroxide. Here, the $d$ value calculated for peak $D_4$ resembled that of $D_\beta$ which is associated with the initial cellulose and not the corresponding reflection in the wool keratin profile. In fact, smaller $d$-spacings were calculated when cellulose dominated in the regenerated blend. This makes sense since compared to keratin; cellulose would have been the major contributor to crystalline *sub*-nanostructures within the samples. In other words, closely packed structures were produced when cellulose is the dominating polymer within these blends. Furthermore, bimodality (peak $G_4$) in the regenerated sample profiles contains the sharpest reflection intensities; this doublet had calculated $d$ values of 0.45 and 0.40 nm for the first and second peaks, respectively. This means that the most compact subnanostructure was only calculated for the samples made from 25% hydrogen peroxide.

The periodicity located in the SAXS data for the initial wool keratin seems to have been lost in all of the regenerated biomaterial samples. A shoulder reflection, which is most likely representative of the nanophase separation between polymer morphologies, appears in the 75% wool keratin profiles: specifically, the 1% ethanol and the 25% hydrogen peroxide coagulated samples. This reflection was also seen in all 25% wool keratin samples with the exception of the film coagulated in 25% hydrogen peroxide. This shoulder, labeled as $A_n$, has $d$ values similar to the initial Avicel cellulose peak, $A_\beta$. Therefore, it is theorized that cellulose greatly influences the manipulation of a blend's nanophase separation upon material fabrication. However, it must be noted that the $d$ values were larger in all regenerated samples ($d$ = 4.21−4.87 nm) than that of initial cellulose ($d$ = 3.22 nm). This means that wool keratin still played a significant role in shifting the scattering vector to mostly lower $q$ values within the SAXS data, and thus, larger interplanar spacing values were calculated for the biomaterial blends. Various reflections representative of initial wool keratin and cellulose appeared in the regenerated samples containing both polymers, and specific regions for these reflections have been denoted to further the study of the nanostructure morphology of biocomposite blends.

Figure 9 shows a possible schematic representation of the effect of hydrogen peroxide in the fabrication process. This figure was modeled after a study from Vu et al.[41] In this figure, the first row shows the initial stage of cellulose and keratin azure during dissolution in ionic liquids. In this case both materials completely dissolve in ionic liquids. Upon coagulation, phase separation quickly occurs as both the cellulose and keratin structures reorganize. This structural reorganization is dependent upon both material content and coagulation agent type. As shown in the schematic, $\beta$ sheet formation is affected by both material composition and hydrogen peroxide content. The same can be said for the cellulose in terms of cellulose crystallites as shown in the X-ray scattering as a function of hydrogen peroxide content. After a period of 48 h during coagulation, the regenerated material forms into an imperfect gelation in which both materials are blended by various molecular interactions. These molecular interactions determine the final morpholog and thermal and physicochemical properties as demonstrated in the various results.

## CONCLUSIONS

Through the various percent compositions and coagulation agents used in this study, the resulting structural, thermal, and morphological properties of the wool keratin-cellulose biocomposite films were altered, compared to that of the



https://doi.org/10.1021/acsmaterialsau.1c00016
ACS Mater. Au 2022, 2, 21−32

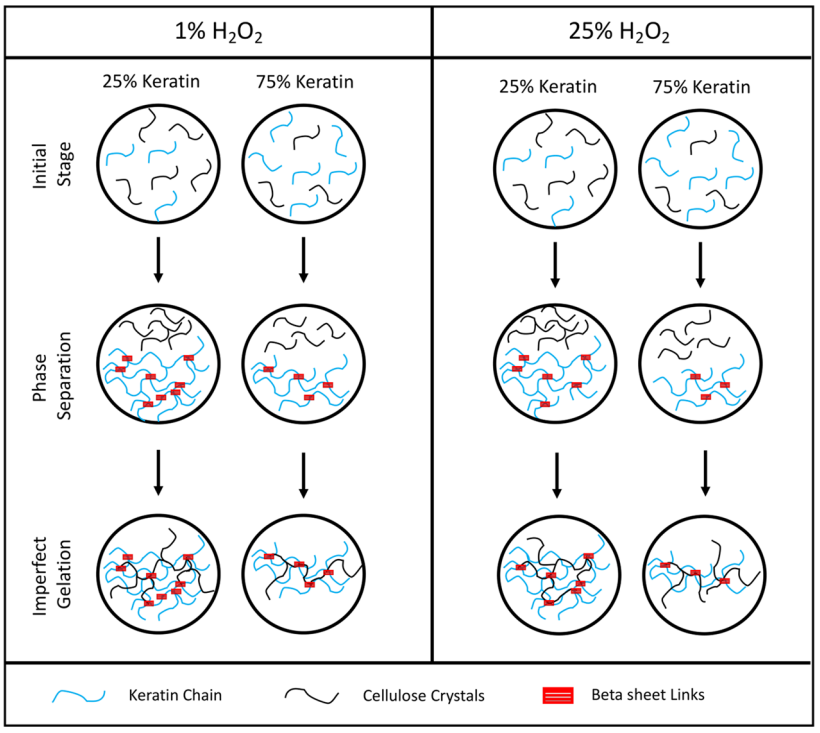


**Figure 9.** Structural mechanism of the natural self-assembled wool keratin/cellulose films, both 25% and 75% wool keratin, coagulated with 1% and 25% hydrogen peroxide.

initial protein and polysaccharide samples. FTIR showed the regeneration of the initial samples and the variations in the protein secondary structure of the amide I region. As the structure of wool keratin is primarily composed of the $\alpha$-keratin type, the secondary structures within the protein contributes to the amorphous regions while the formation of crystalline regions is primarily due to the cellulose microcrystals and the fabrication method. This study confirmed previous studies that the percentage of ethanol influenced the resulting percentage of $\beta$-sheets and crystalline areas within the sample. Another trend seen within the secondary structures was that when there was a higher percentage of protein present within the sample, there was an overall increase in the $\beta$-sheets. Through the analysis of the thermal properties, the regenerated samples' thermograms were shown to have a decreased thermal stability as compared to the initial samples. The protein composition percentages also had an effect as the 25% wool keratin had a bimodal thermogram and the 75% wool keratin had a unimodal thermogram. Also, the increase in coagulation concentration resulted in an increased onset temperature. The DSC analysis of the glass transition temperatures in the different coagulation agents showed that samples coagulated in ethanol had less variation than the hydrogen peroxide films. X-ray 1-D profiles showed that the scattering vector for peaks representative of semicrystalline regions within the initial wool keratin and cellulose shifted in the profiles of the regenerated samples. These parameter changes in the fabrication, i.e., ethanol vs hydrogen peroxide as the coagulant, also affected the nanophase separation when compared to the initial samples. The resulting crystallinity of cellulose was not affected by the protein structure but only by the post-treatment of the biocomposites. The different molecular interactions can give insight into the morphological, thermal, and mechanical properties. Analysis of all aforementioned characterization tests further confirmed that the morphologies of wool keratin to cellulose regenerated films were influenced by both the polymer composition ratio as well as the coagulation agent type. Having an understanding of the different properties as well as the physical and chemical interactions within the biocomposite films can lead to a multitude of versatile applications.

## ■ ASSOCIATED CONTENT

### Supporting Information

The Supporting Information is available free of charge at https://pubs.acs.org/doi/10.1021/acsmaterialsau.1c00016.

Figure S-1 showing the profiles of the different amide I bands located from 1705−1595 $cm^{-1}$ of 25% wool keratin and 75% cellulose and 75% wool keratin and 25% cellulose and the differences between the amide I regions (PDF)

## ■ AUTHOR INFORMATION

### Corresponding Author

**David Salas-de la Cruz** − *Center of Computational and Integrative Biology and Department of Chemistry, Rutgers University—Camden, Camden, New Jersey 08102, United States;* orcid.org/0000-0002-5835-4325; Email: david.salas@camden.rutgers.edu

### Authors

**Karleena Rybacki** − *Center of Computational and Integrative Biology, Rutgers University—Camden, Camden, New Jersey 08102, United States;* orcid.org/0000-0002-6609-6573

**Stacy A. Love** − *Center of Computational and Integrative Biology, Rutgers University—Camden, Camden, New Jersey 08102, United States*



https://doi.org/10.1021/acsmaterialsau.1c00016
ACS Mater. Au 2022, 2, 21−32

**Bailey Blessing** − *Department of Chemistry, Rutgers University—Camden, Camden, New Jersey 08102, United States*
**Abneris Morales** − *Department of Chemistry, Rutgers University—Camden, Camden, New Jersey 08102, United States*
**Emily McDermott** − *Department of Chemistry, Rutgers University—Camden, Camden, New Jersey 08102, United States*
**Kaylyn Cai** − *Department of Chemical and Biochemical Engineering, Rutgers University—New Brunswick, New Brunswick, New Jersey 08901, United States*
**Xiao Hu** − *Department of Physics and Astronomy, Rowan University, Glassboro, New Jersey 08102, United States;* orcid.org/0000-0002-2579-2820

Complete contact information is available at: https://pubs.acs.org/10.1021/acsmaterialsau.1c00016

## Notes

The authors declare no competing financial interest.

## ■ ACKNOWLEDGMENTS

We want to acknowledge the funding provided by The National Science Foundation Grant (DBI-1559868, DMR 1809354, and DMR 1809541), Rutgers University—Camden Center of Computational and Integrative Biology (CCIB), Rutgers University—Camden Laboratory Start-up funds, the State of New Jersey ELF Grant to Rutgers—Chemistry. Thank You to Rouwaidia Nitiema, Gettysburg College, Gettysburg, PA, India Jackson, Rutgers University—New Brunswick, New Brunswick, NJ, and Ashley Rivera-Galletti, Rowan University, Glassboro, NJ. X-ray Scattering System (DEXS) is supported by NSF-MRSEC (17-20530), NSF-MRI (17-25969), ARO DURIP (W911NF-17-1-02822), and the University of Pennsylvania.

## ■ REFERENCES

(1) Stanton, J.; Xue, Y.; Pandher, P.; Malek, L.; Brown, T.; Hu, X.; Salas-de la Cruz, D. Impact of ionic liquid type on the structure, morphology and properties of silk-cellulose biocomposite materials. *Int. J. Biol. Macromol.* **2018**, *108*, 333−341.
(2) Love, S. A.; Popov, E.; Rybacki, K.; Hu, X.; Salas-de la Cruz, D. Facile treatment to fine-tune cellulose crystals in cellulose-silk biocomposites through hydrogen peroxide. *Int. J. Biol. Macromol.* **2020**, *147*, 569−575.
(3) Sharma, S.; Kumar, A. *Keratin as a Protein Biopolymer*; Springer: 2019.
(4) Blessing, B.; Trout, C.; Morales, A.; Rybacki, K.; Love, S. A; Lamoureux, G.; O'Malley, S. M; Hu, X.; Salas-de la Cruz, D. Morphology and ionic conductivity relationship in silk/cellulose biocomposites. *Polym. Int.* **2019**, *68* (9), 1580−1590.
(5) O'brien, F. J. Biomaterials & scaffolds for tissue engineering. *Mater. Today* **2011**, *14* (3), 88−95.
(6) Salama, A.; El-Sakhawy, M. Regenerated cellulose/wool blend enhanced biomimetic hydroxyapatite mineralization. *Int. J. Biol. Macromol.* **2016**, *92*, 920−925.
(7) Jia, X.; Wang, C.; Zhao, C.; Ge, Y.; Wallace, G. G. Towards Biodegradable Mg-Air Bioelectric Batteries Composed of Silk Fibroin-Polypyrrole Film. *Adv. Funct. Mater.* **2016**, *26*, 1454−1462.
(8) Jia, X.; Wang, C.; Ranganathan, V.; Napier, B.; Yu, C.; Chao, Y.; Forsyth, M.; Omenetto, F. G.; MacFarlane, D. R.; Wallace, G. G. A biodegradable thin-film magnesium primary battery using silk fibroin−ionic liquid polymer electrolyte. *ACS Energy Letters* **2017**, *2* (4), 831−836.
(9) Cui, L.; Gong, J.; Fan, X.; Wang, P.; Wang, Q.; Qiu, Y. Transglutaminase□modified wool keratin film and its potential application in tissue engineering. *Engineering in Life Sciences* **2013**, *13* (2), 149−155.
(10) Freddi, G.; Romanò, M.; Massafra, M. R.; Tsukada, M. Silk fibroin/cellulose blend films: preparation, structure, and physical properties. *J. Appl. Polym. Sci.* **1995**, *56* (12), 1537−1545.
(11) Zhou, L.; Wang, Q.; Wen, J.; Chen, X.; Shao, Z. Preparation and characterization of transparent silk fibroin/cellulose blend films. *Polymer* **2013**, *54* (18), 5035−5042.
(12) Wongpanit, P.; Sanchavanakit, N.; Pavasant, P.; Bunaprasert, T.; Tabata, Y.; Rujiravanit, R. Preparation and characterization of chitin whisker-reinforced silk fibroin nanocomposite sponges. *Eur. Polym. J.* **2007**, *43* (10), 4123−4135.
(13) Tran, C. D.; Mututuvari, T. M. Cellulose, chitosan and keratin composite materials: Facile and recyclable synthesis, conformation and properties. *ACS Sustainable Chem. Eng.* **2016**, *4* (3), 1850−1861.
(14) Boy, R.; Narayanan, G.; Chung, C.-C.; Kotek, R. Novel cellulose-collagen blend biofibers prepared from an amine/salt solvent system. *Int. J. Biol. Macromol.* **2016**, *92*, 1197−1204.
(15) Takada, A.; Kadokawa, J.-i. Fabrication and characterization of polysaccharide ion gels with ionic liquids and their further conversion into value-added sustainable materials. *Biomolecules* **2015**, *5* (1), 244−262.
(16) Kadokawa, J.-i.; Murakami, M.-a.; Takegawa, A.; Kaneko, Y. Preparation of cellulose−starch composite gel and fibrous material from a mixture of the polysaccharides in ionic liquid. *Carbohydr. Polym.* **2009**, *75* (1), 180−183.
(17) Singh, S.; Simmons, B. A.; Vogel, K. P. Visualization of biomass solubilization and cellulose regeneration during ionic liquid pretreatment of switchgrass. *Biotechnol. Bioeng.* **2009**, *104* (1), 68−75.
(18) Badgujar, K. C.; Bhanage, B. M. Factors governing dissolution process of lignocellulosic biomass in ionic liquid: current status, overview and challenges. *Bioresour. Technol.* **2015**, *178*, 2−18.
(19) Stoddart, A.; Cleave, V. The evolution of biomaterials. *Nat. Mater.* **2009**, *8* (6), 444−445.
(20) Van Vlierberghe, S.; Dubruel, P.; Schacht, E. Biopolymer-based hydrogels as scaffolds for tissue engineering applications: a review. *Biomacromolecules* **2011**, *12* (5), 1387−1408.
(21) Singh, N.; Rahatekar, S. S.; Koziol, K. K.; Ng, T. S.; Patil, A. J.; Mann, S.; Hollander, A. P.; Kafienah, W. Directing chondrogenesis of stem cells with specific blends of cellulose and silk. *Biomacromolecules* **2013**, *14* (5), 1287−1298.
(22) Feng, Y.; Li, X.; Li, M.; Ye, D.; Zhang, Q.; You, R.; Xu, W. Facile preparation of biocompatible silk fibroin/cellulose nanocomposite films with high mechanical performance. *ACS Sustainable Chem. Eng.* **2017**, *5* (7), 6227−6236.
(23) Guzman-Puyol, S.; Heredia-Guerrero, J. A.; Ceseracciu, L.; Hajiali, H.; Canale, C.; Scarpellini, A.; Cingolani, R.; Bayer, I. S.; Athanassiou, A.; Mele, E. Low-cost and effective fabrication of biocompatible nanofibers from silk and cellulose-rich materials. *ACS Biomater. Sci. Eng.* **2016**, *2* (4), 526−534.
(24) Dong, X.; Zhao, Q.; Xiao, L.; Lu, Q.; Kaplan, D. L. Amorphous silk nanofiber solutions for fabricating silk-based functional materials. *Biomacromolecules* **2016**, *17* (9), 3000−3006.
(25) Sharma, S.; Gupta, A. Sustainable management of keratin waste biomass: applications and future perspectives. *Braz. Arch. Biol. Technol.* **2016**, DOI: 10.1590/1678-4324-2016150684.
(26) Reichl, S.; Borrelli, M.; Geerling, G. Keratin films for ocular surface reconstruction. *Biomaterials* **2011**, *32* (13), 3375−3386.
(27) Wu, M.; Shen, S.; Yang, X.; Tang, R. In *Preparation and study on the structure of keratin/PVA membrane containing wool fibers*; IOP Conference Series: Materials Science and Engineering; IOP Publishing: 2017; p 042030.
(28) Tran, C. D.; Prosenc, F.; Franko, M.; Benzi, G. Synthesis, structure and antimicrobial property of green composites from cellulose, wool, hair and chicken feather. *Carbohydr. Polym.* **2016**, *151*, 1269−1276.

(29) Scott, J.; Untereiner, W. Determination of keratin degradation by fungi using keratin azure. *Med. Mycol.* **2004**, *42* (3), 239−246.
(30) Greenwold, M. J.; Bao, W.; Jarvis, E. D.; Hu, H.; Li, C.; Gilbert, M. T. P.; Zhang, G.; Sawyer, R. H. Dynamic evolution of the alpha ($\alpha$) and beta ($\beta$) keratins has accompanied integument diversification and the adaptation of birds into novel lifestyles. *BMC Evol. Biol.* **2014**, *14* (1), 249.
(31) McKittrick, J.; Chen, P.-Y.; Bodde, S.; Yang, W.; Novitskaya, E.; Meyers, M. The structure, functions, and mechanical properties of keratin. *JOM* **2012**, *64* (4), 449−468.
(32) Wang, B.; Yang, W.; McKittrick, J.; Meyers, M. A. Keratin: Structure, mechanical properties, occurrence in biological organisms, and efforts at bioinspiration. *Prog. Mater. Sci.* **2016**, *76*, 229−318.
(33) Kooshamoghadam, N.; Zohoori, S.; Bekrani, M.; Shahsavari, S.; Talebikatieklahijany, R. Enhancing physical properties of viscose by preparing Viscose/Keratin/Nano ZnO composite Fabric. *J. Nat. Fibers* **2021**, 1−8.
(34) Stanton, J.; Xue, Y.; Waters, J. C.; Lewis, A.; Cowan, D.; Hu, X.; Salas-de la Cruz, D. Structure−property relationships of blended polysaccharide and protein biomaterials in ionic liquid. *Cellulose* **2017**, *24* (4), 1775−1789.
(35) Pinkert, A.; Marsh, K. N.; Pang, S.; Staiger, M. P. Ionic liquids and their interaction with cellulose. *Chem. Rev.* **2009**, *109* (12), 6712−6728.
(36) Idris, A.; Vijayaraghavan, R.; Rana, U. A.; Patti, A. F.; Macfarlane, D. R. Dissolution and regeneration of wool keratin in ionic liquids. *Green Chem.* **2014**, *16* (5), 2857−2864.
(37) Li, Y.; Wang, J.; Liu, X.; Zhang, S. Towards a molecular understanding of cellulose dissolution in ionic liquids: anion/cation effect, synergistic mechanism and physicochemical aspects. *Chemical science* **2018**, *9* (17), 4027−4043.
(38) Blessing, B.; Trout, C.; Morales, A.; Rybacki, K.; Love, S. A.; Lamoureux, G.; O'malley, S. M.; Hu, X.; Salas-De la Cruz, D. The impact of composition and morphology on ionic conductivity of silk/cellulose bio-composites fabricated from ionic liquid and varying percentages of coagulation agents. *Int. J. Mol. Sci.* **2020**, *21* (13), 4695.
(39) Xue, Y.; Jao, D.; Hu, W.; Hu, X. Silk-silk blend materials. *J. Therm. Anal. Calorim.* **2017**, *127* (1), 915−921.
(40) Hu, X.; Kaplan, D.; Cebe, P. Determining beta-sheet crystallinity in fibrous proteins by thermal analysis and infrared spectroscopy. *Macromolecules* **2006**, *39* (18), 6161−6170.
(41) Vu, T.; Xue, Y.; Vuong, T.; Erbe, M.; Bennet, C.; Palazzo, B.; Popielski, L.; Rodriguez, N.; Hu, X. Comparative study of ultrasonication-induced and naturally self-assembled silk fibroin-wool keratin hydrogel biomaterials. *Int. J. Mol. Sci.* **2016**, *17* (9), 1497.
(42) Li, R.; Wang, D. Preparation of regenerated wool keratin films from wool keratin−ionic liquid solutions. *J. Appl. Polym. Sci.* **2013**, *127* (4), 2648−2653.


https://doi.org/10.1021/acsmaterialsau.1c00016
*ACS Mater. Au* 2022, 2, 21−32